Dry sliding wear behaviour of oil jet peened aluminium alloy, AA6063-T6

N Arun Prakash[1], **R Gnanamoorthy**[2*], and **M Kamaraj**[3]
[1]Department of Mechanical Engineering, Indian Institute of Technology Madras, Chennai, India
[2]Indian Institute of Information Technology, Design and Manufacturing, (IIITD&M), IIT Madras Campus, Kancheepuram, Chennai, India
[3]Department of Metallurgical and Materials Engineering, Indian Institute of Technology Madras, Chennai, India

The manuscript was received on 12 January 2010 and was accepted after revision for publication on 7 June 2010.

DOI: 10.1243/13506501JET781

Abstract: Oil jet peening makes use of high-pressure oil jet to impart compressive residual stresses on the surface of metallic materials in order to improve the surface properties. This article reports the dry sliding wear characteristics of oil jet peened aluminium alloy, AA6063-T6. The presence of compressive residual stress and high hardness improves the wear resistance of oil jet peened surfaces. Changes in the hardness, surface morphology, and residual stress distribution due to peening affect the tribological behaviour. The initial and steady-state coefficient of friction are less in the treated samples compared to untreated samples. The scanning electron microscope images of the worn surfaces reveal the dominant adhesive and mild abrasive form of wear.

Keywords: oil jet peening, aluminium alloy, sliding friction

1 INTRODUCTION

Aluminium alloys are extensively used in automobile and aerospace industries due to their high strength-to-weight ratio, good ductility, and excellent corrosion resistance. An economical approach to use aluminium alloys for application that require high fatigue strength and wear resistance is to improve their surface strength. Surface properties can be improved by changing the composition or microstructure gradually with depth by chemical, thermochemical, thermal, or mechanical treatments. Introduction of compressive residual stress field is one potential means of increasing the resistance to crack initiation and propagation in machine components subjected to cyclic loading. Shot peening, water jet peening, laser shock peening, deep rolling, low plasticity burnishing, and ultrasonic peening are a few surface deformation processes used to impart beneficial compressive residual stress field on metallic surfaces. A surface enhancement process, namely oil jet peening (OJP), was developed for imparting the compressive residual stresses on metallic materials [**1**]. In this process, high-velocity hydraulic oil is made to impinge through a nozzle on the material to be peened. The process improves the flexural fatigue strength of the aluminium alloy [**2**] and steel [**3**].

The wear behaviour of surface-modified aluminium alloys is widely studied [**4**–**8**]. The artificially age-hardened aluminium alloy, AA6063, showed better wear resistance compared to as-cast aluminium samples [**4**]. The retrogression- and reaging-treated aluminium alloy, 7039, exhibited good dry sliding and cavitation erosion–corrosion wear resistance than treated aluminium alloy, AA7039-T6 [**5**]. The wear rate of near-eutectic Al–Si alloy was found to depend on the sliding speed [**6**] and the wear mechanism was reported to change with sliding speed. Many researchers have also reported a significant effect of normal load on the wear rate [**7**]. Laser shock processing reduces the wear rate of 6061-T6 aluminium alloy due to the presence of compressive residual stresses [**8**]. The wear rate was found to be less at high pulse densities. The nanocrystalline surface layer produced in aluminium alloy by controlled ball impact treatment showed lower initial and steady-state friction

*Corresponding author: Indian Institute of Information Technology, Design and Manufacturing, (IIITD&M), IIT Madras Campus, Kancheepuram, Chennai 600036, India.
email: gmoorthy@iitm.ac.in

coefficient compared to coarse grained sample [**9**]. The improvement in the wear rate of the nanocrystalline surface layer is attributed to the improved surface strength, presence of compressive residual stress, and associated grain refinement.

This article demonstrates the effect of OJP on the tribological characteristics of aluminium alloy, AA6063-T6, under dry sliding conditions. The effect of applied load and peening conditions on the friction and wear characteristics is presented. The wear mechanisms of the peened aluminium alloy are discussed.

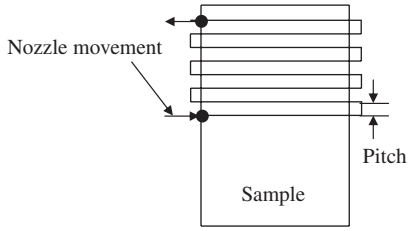

Fig. 1 Schematic diagram showing the movement of nozzle. The pitch is selected to impart complete coverage

2 MATERIAL AND EXPERIMENTAL DETAILS

The material used is aluminium alloy, AA6063-T6. Specimens of dimensions, 25 mm × 30 mm (surface area), were machined from 6 mm thick plate. Specimens were polished using different grades of silicon carbide abrasive paper up to a grit size #1200 and then polished using fine alumina powder prior to the treatment. A surface roughness of $0.1 \pm 0.02\,\mu$m (R_a) was maintained in the samples before OJP. Specimens were ultrasonically cleaned in acetone before and after the treatment.

The OJP unit, designed and developed consists of nozzle drive unit, nozzle, specimen drive unit, and peening chamber [**1**]. The test rig permits different nozzle-travelling velocities ranging from 0.005 to 5 mm/s using a computer-controlled servo motor [**1**, **3**]. The nozzle-travelling velocity decides the peening coverage, intensity of peening, and surface roughness and affects the surface properties. Specimens were oil jet peened at a constant oil supply pressure of 50 MPa and stand-off distance (SOD) of 25 mm. A cylindrical nozzle of throat diameter of 0.25 mm and length of 2 mm is used. The angle of attack is 90° and the pitch is 0.25 mm. Single pass peening pattern was followed for entire test. This pattern ensured full coverage on the specimen surface. The samples were peened at different transverse nozzle-travelling velocities, 0.5, 1, 1.5, and 2 mm/s to attain different peening intensities and coverage [**1**, **3**]. The oil used for peening is anti-wear hydraulic oil grade, ISO VG 68. Table 1 shows the chemical composition (in wt%) of test material. Figure 1 shows the schematic of the oil jet movement.

The microstructure of the treated surface was characterized using optical microscope, scanning electron microscope, and transmission electron microscope (TEM). The average grain size of the untreated sample determined by optical microscope is ∼410 μm [**10**]. The indentation hardness and residual stress of the treated surface were evaluated using a dynamic ultra micro-hardness tester using Berkovich indenter. The grain size of the treated surface is quantified using X-ray diffraction (XRD) analysis and TEM. Surface roughness of the treated and untreated samples was measured using a profilometer.

Table 1 Chemical composition of aluminium alloy, AA6063-T6 (in wt%)

Cu	Mg	Si	Fe	Mn	Zn	Ti	Cr	Al
0.1	0.4–0.9	0.3–0.7	0.6	0.3	0.2	0.2	0.1	Balance

Sliding wear tests were carried out in a reciprocating sliding wear test rig developed in-house. The coefficient of friction and wear rate of test materials were evaluated by sliding them against a high-carbon high-chromium hardened steel ball of 10 mm diameter. The hardness of the steel ball is 60 ± 2 HRC (Rockwell hardness in C scale). The sliding wear tests of the peened samples were performed in the as-peened conditions. All tests were performed at room temperature in laboratory atmosphere neglecting the effect of contact temperature between the mating members. Tests were conducted at different normal loads, 10, 20, and 30 N, at a constant stroke length of 5 mm. All tests were carried out at a sliding velocity of 9.26×10^{-3} m/s up to a sliding distance of 150 m. The friction force measured using a precision load cell was continuously recorded using a personal computer-based data acquisition system. For each cycle of reciprocating sliding, ten data points of friction force values were acquired. The coefficient of friction was calculated from the mean friction force values obtained in a cycle divided by the corresponding normal force applied. The weight of the specimen was measured before and after the test using a precision electronic balance of 0.01 mg accuracy from which the weight loss and wear volume were evaluated. The specific wear rate, K, reported is estimated according to the following equation

$$K = \frac{V}{PS} \tag{1}$$

where V is the wear volume of the sample, P is the applied normal load, and S is the sliding distance. At least three replicate sliding tests were carried out at each test condition. The friction coefficient and wear rate reported are the average of three replicate test data. The percentage variation of each experimental value from their average value is shown as the error bar. The variation in the data was within ±6 per cent. Basic wear curves (weight loss versus applied

load) were obtained for the peened and unpeened conditions at various loads and subsequently wear rates were calculated. The wear profile was studied using a profilometer. The morphology and chemical composition of the worn surface at different peening conditions were examined using a scanning electron microscope.

3 RESULTS AND DISCUSSION

3.1 Material characterization

The OJP process involves impingement of a high-pressure oil jet on the target surface to be peened. During peening, each drop of oil jet generates a large impulse pressure and shear stresses and causes severe plastic deformation. For a single oil drop impact on a stationary elastic surface, the impact pressure can be approximated as [**11**]

$$P_{\text{imp}} = \frac{C_v C_1 d_n^2 \sqrt{2\rho_1 P_0}}{(d_n + 2\text{SOD}\tan(\theta/2))^2}\left(\frac{\rho_2 C_2}{\rho_1 C_1 + \rho_2 C_2}\right) \quad (2)$$

where C_v is the coefficient of nozzle ($= 0.98$), ρ_1 is the density of oil, ρ_2 is the density of target material, d_n is the nozzle throat diameter, SOD is the stand-off distance, P_0 is the operating oil pressure, θ is the diverging angle of the oil jet droplet, C_1 is the velocity of sound in oil, and C_2 is the velocity of sound in target material. The impact pressure exerted on the target material due to oil jet impingement is calculated to be 270 MPa for the SOD of 25 mm [**11**]. The surface of material is subjected to repeated impacts and impact pressure is higher than yield stress of aluminium alloy used ($\sigma_y = 150$ MPa). This causes a severe plastic deformation at the surface of the peened target. The impact pressure depends on the normal component of the impact velocity. It is assumed that during peening operation, the motion of oil jet produces uniform pressure across the contact area. To consider the phenomenon of the full stream of oil jet, it is assumed that the target surface is repeatedly struck by multiple impacts of single oil droplet. The exposure time of the target (t_p) surface by repeated impacts over a contact area is given as [**12**]

$$t_p = \frac{(d_n + 2\text{SOD}\tan(\theta/2))}{u} \quad (3)$$

where u is the nozzle-travelling velocity.

The severe surface plastic deformation of oil jet peened aluminium alloy is quantified based on the microstructural changes occur during the treatment. As a result of this, high-density dislocations are generated which on repeated impacts annihilate and recombine to form smaller grains. Further plastic straining refines the grain size and results in ultrafine grain structure. The average grain size of the treated surface layer measured using TEM micrographs are 210, 285, and 295 nm for the samples peened at 0.5, 1, and 2 mm/s, respectively [**10**]. Studies reveal the polycrystalline nature of the material and the random orientation of the constitute grain [**10**]. The average grain size of the treated samples is estimated from the line broadening of XRD peaks using the Scherrer and Wilson method and is reported in Table 2.

Hardness and residual stress of the treated samples are determined from the load-depth curves obtained from microindentation experiments and reported values are the average of five indentation test data [**13**, **14**]. The indentation hardness of the untreated aluminium sample is 0.58 ± 0.01 GPa. The surface hardness of the treated sample increases approximately by 25 per cent to 45 per cent of unpeened aluminium sample based on the nozzle-travelling velocity. Hardness measurement conducted on the treated samples through the metallographically prepared cross-sectioned specimen revealed the depth of the hardened layer is about $\sim$400 μm depending upon the nozzle-travelling velocity [**10**]. The magnitude of hardness produced by OJP process is high at the surface and decrease with increased distance from the treated surface. The surface compressive residual stress induced is about 72 per cent, 62 per cent, 43 per cent, and 35 per cent of yield strength in the specimen peened at nozzle-travelling velocities 0.5, 1, 1.5, and 2 mm/s, respectively. In the peening conditions investigated, it is observed that the maximum compressive residual stresses were induced below the surface due to increase in the dislocation density. Table 2 shows the grain size calculated from XRD measurement, centre-line average surface roughness (R_a), indentation hardness, compressive residual stress, and surface dislocation density with different nozzle-travelling velocities.

Figure 2 shows the schematic of the microstructure evolution along the depth from the treated surface. At the surface ultrafine grains are formed. As depth below the treated surface increases, a refined structured

Table 2 Characteristics of the treated surfaces [**10**]

Peening condition	Grain size (nm)	Surface roughness, R_a (μm)	Indentation hardness ($\times 10^{-3}$ GPa)	Compressive residual stress (MPa)	Surface dislocation density, p ($\times 10^{15}$ m^{-2})
Peened at 0.5 mm/s	240 ± 5	3.61 ± 0.2	876 ± 12	102 ± 7	13.1
Peened at 1 mm/s	290 ± 8	2.2 ± 0.1	855 ± 10	88 ± 5	11.1
Peened at 1.5 mm/s	346 ± 7	1.31 ± 0.1	820 ± 9	61 ± 4	8.1
Peened at 2 mm/s	391 ± 10	0.82 ± 0.05	732 ± 8	50 ± 3	3.7

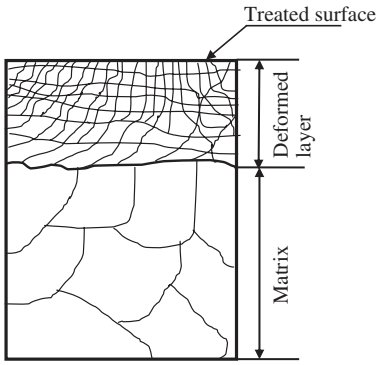

Fig. 2 Schematic illustration of the microstructure evolution along the depth from the treated surface layer

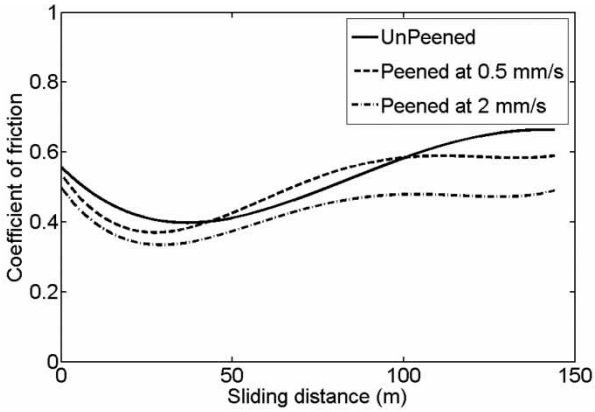

Fig. 3 Variation of the coefficient of friction for the unpeened and peened samples tested at a normal load of 30 N

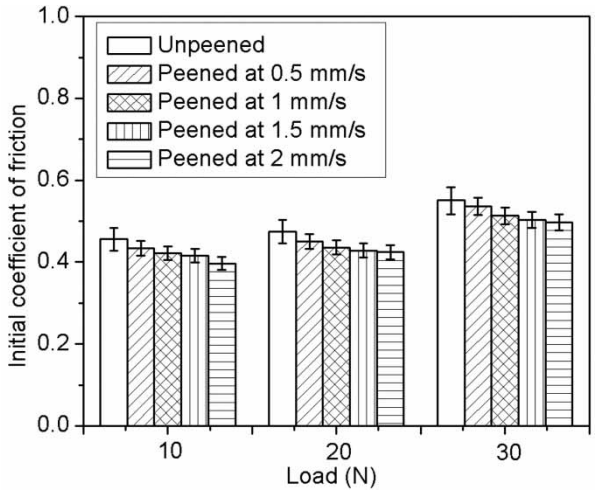

Fig. 4 Initial coefficient of friction plotted against applied load for samples peened at different nozzle-travelling velocities

layer consisting of submicron-sized crystallites or cells separated by either grain boundaries or subboundaries are visible. At a distance from the surface, deformed coarse grains with different dislocation configuration are observed. As oil jet peened surfaces are heavily deformed, grain boundaries of the treated sample are not clearly visible unlike untreated sample. The depth of the deformed layer is not uniform due to variation in orientations of the grains and the heterogeneous nature of the plastic deformation within and between the grains [**10**]. The specimen peened at low nozzle-travelling experiences more number of continuous impacts of the oil droplet resulting in improved hardness, compressive residual stress, grain refinement, increased depth of hardened layer, and increased dislocation density.

3.2 Coefficient of friction

Typical variation of coefficient of friction quantified from the dry sliding tests conducted at an applied normal load of 30 N for both unpeened and peened samples is shown in Fig. 3. The coefficient of friction presented in Fig. 3 is the mean value of the friction coefficient over the sliding distance. During the run-in period, smoothening of the surface occurs which leads to a decrease in the coefficient of friction. The presence of debris generated in the sliding path causes a rise in the coefficient of friction with further sliding. Similar variation in the friction coefficient was observed in all the tests conducted at different normal loads.

The friction force measured during the initial stage (i.e. average value of first ten cycles) of the experiment is termed as initial coefficient of friction. Initial coefficient of friction depends on the change in the geometry of the sliding surfaces, surface roughness of mating surfaces, and physicomechanical properties of the surface layers of the material. The initial coefficient of friction measured during the tests conducted at different normal loads for various peening conditions investigated is shown in Fig. 4. The initial coefficient of friction at the beginning of the test ranges between 0.40 and 0.54 for all the samples investigated. Compared with the conventional coarse-grained (unpeened) sample, oil jet peened samples exhibited low initial coefficient of friction at all normal loads. The low initial friction coefficient in the peened samples may be attributed to the formation of ultrafine grains in the surface layers and increased substrate strength. In rough surfaces, severe asperity interlocking during the initial stages of running causes a high initial coefficient of friction.

After initial perturbations, the friction force reaches a condition that is referred here as the steady-state coefficient of friction, in which the various parameters influencing friction have reached a steady state. In the present context, steady-state coefficient of friction is that condition of a given tribosystem in which the average kinetic friction coefficient, wear rate, and surface roughness have reached and maintained a relatively constant level. The steady-state coefficient

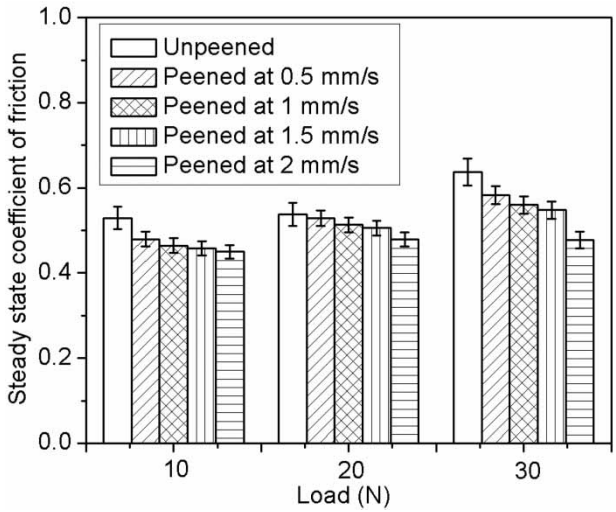

Fig. 5 Steady-state coefficient of friction plotted against applied load for samples peened at different nozzle-travelling velocities

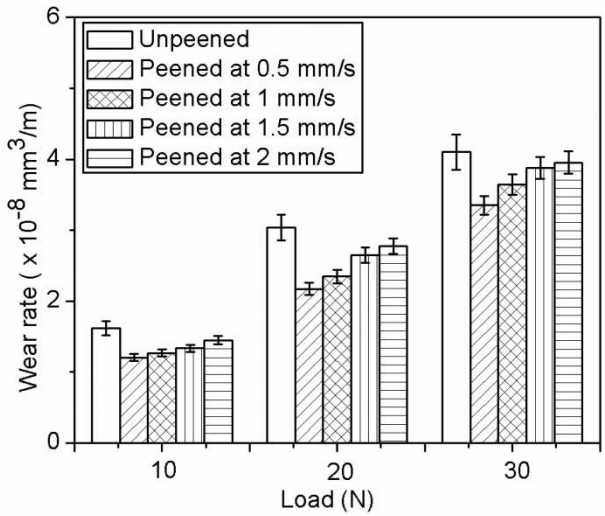

Fig. 6 Wear rate for the samples tested at different applied loads and varying nozzle-travelling velocities

of friction of the test materials at different normal loads is shown in Fig. 5. The steady-state coefficient of friction depends on the texture of the material. The highly deformed or work hardened layer developed during sliding compared to the initial crystallographic structure affects the friction characteristics. As the applied normal load increases, due to the increase in the apparent area of contact more interfacial bonds develop resulting in an increased steady-state friction coefficient. Wear of the asperities results in more compatibility between the mating surfaces and the coefficient of friction reaches a steady state. The surface roughness has a less effect on the steady-state coefficient of friction, since the asperities were already smoothened during the process.

3.3 Wear rate

In general, the wear is more in rough surfaces [**8**]. Figure 6 shows the wear rate in the samples tested at different applied normal loads for the material treated at various nozzle-travelling velocities. In the present study, the increase in the surface roughness due to the low nozzle-travelling velocity did not imply an increase in wear rate, because the residual stress present in the peened samples dominate the wear process. The wear rate is less in peened specimens compared to unpeened specimens indicating the effectiveness of the OJP process in improving the dry sliding wear characteristics of AA6063-T6 alloy. The wear rate increases as the load, grain size, and nozzle-travelling velocity increase. The presence of compressive residual stress and hardness also influence the wear rate. Materials with high surface hardness exhibit a low wear rate. Wear debris formation is associated with the crack initiation and propagation.

The presence of compressive residual stress delays the crack initiation and propagation, and the amount of residual stress induced in the sample determines the wear resistance. At low applied normal loads, metal-to-metal contact (i.e. apparent area of contact) and stress induced are less and the rate of wear is minimal. During sliding wear tests, the surface and subsurface of the sample are subjected to alternate tensile and compressive stresses. Severe localized plastic deformation and shear strains in the worn surface at high loads give rise to the formation of cracks, which propagate subsequently to cause spalling and increased wear rate. The significant improvement in the wear resistance of the oil jet peened samples can be attributed to the strong surface layer with fine grain crystalline structure, gradient variation in the microstructure, and mechanical properties along the depth from the top surface [**10**].

The wear scar dimension was uniform along the length of the sliding. As the normal load increases, the contact pressure and contact radius increases resulting in increase in area of contact and depth of the wear scar along the sliding direction in reciprocating sliding wear. The wear depth of the treated samples is lower compared to the untreated samples. This is mainly attributed to increased surface hardness with associated grain refinement.

3.4 Wear mechanism

The severe plastic deformation due to unlubricated dry sliding conditions causes microstructural changes near the surface. In addition, the continuous reciprocating sliding exposes the fresh surface, which gets oxidized subsequently. Further sliding results in the removal of oxide layers formed. The presence of oxide

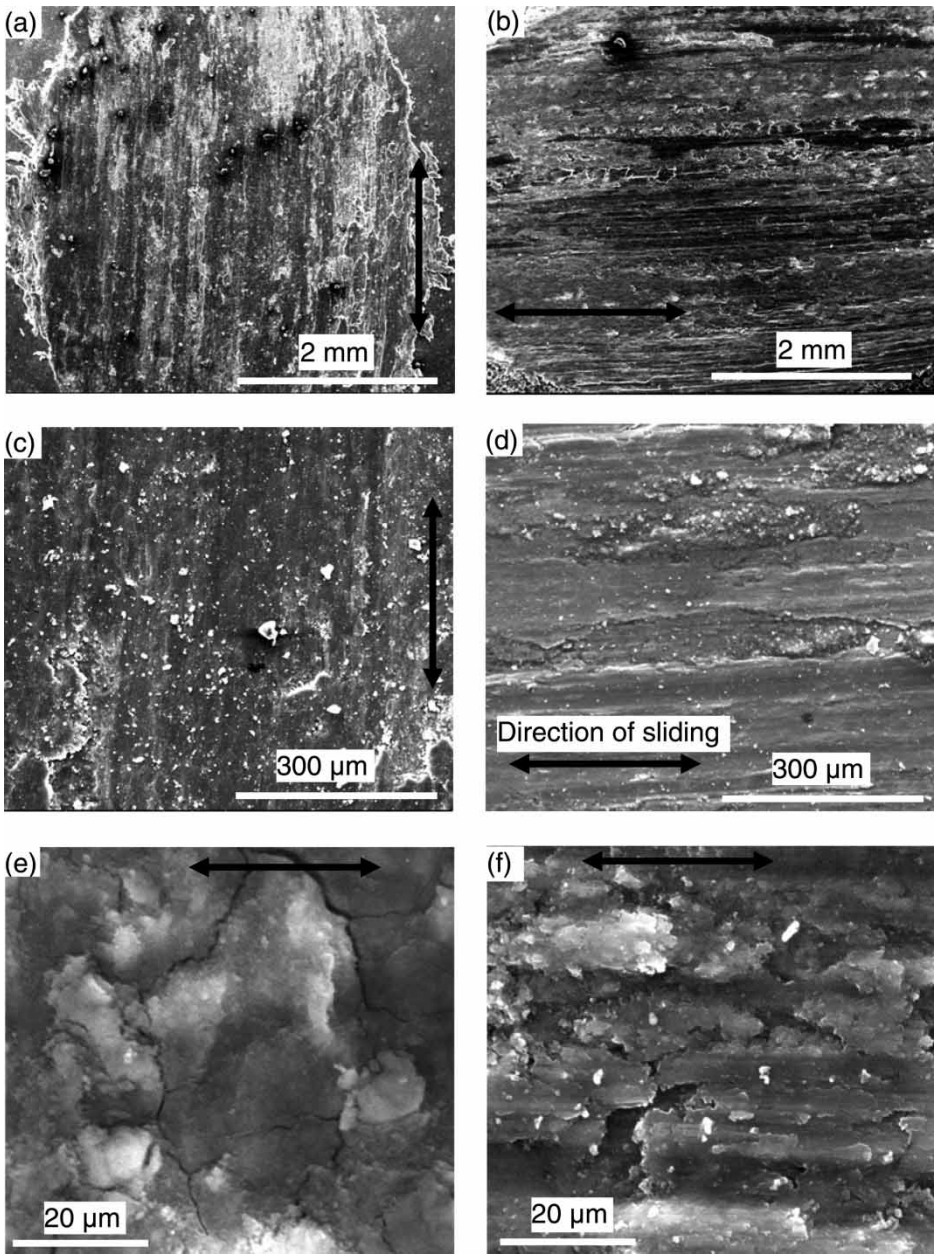

Fig. 7 Worn surface morphology of the tested samples at a load of 30 N: (a) and (c) unpeened sample, peened samples; (b) and (d) at 2 mm/s; (e) and (f) at 1 mm/s; (a) and (b) adhesive and mild abrasive wear; (c) and (d) appearance of large cavities in the wear track; (e) delamination cracks; and (f) delamination with local discontinuity

particles, which are abrasive in nature, acts as a third-body particle and affects the wear rate. Figure 7 shows wear surface morphology of the unpeened and peened samples. The worn surface of the sample shows wear scars, craters, and oxides. The oxide debris formed during the sliding wear process gets accumulated on both sides and in the wear track. Figures 7(a) and (b) indicate the presence of dominant adhesive and abrasive mechanisms in the sample peened at 2 mm/s and unpeened sample tested at an applied load of 30 N. As the load increases, severe localized plastic deformation occurs in the surface and subsurface resulting in dominant adhesive and mild abrasive wear. Figures 7(c) and (d) reveal the appearance of large cavities in the wear track at an applied load of 30 N for the sample peened at 2 mm/s and unpeened sample. The occurrence of delamination cracks (Fig. 7(e)) and delamination with local discontinuity (Fig. 7(f)) on the tested surface were also observed.

The untreated sample shows high plasticity and high rate of wear. The heat generated during the sliding action under unlubricated conditions result in the formation of contact patches. The energy dispersive spectroscopy (EDS) analysis conducted indicates

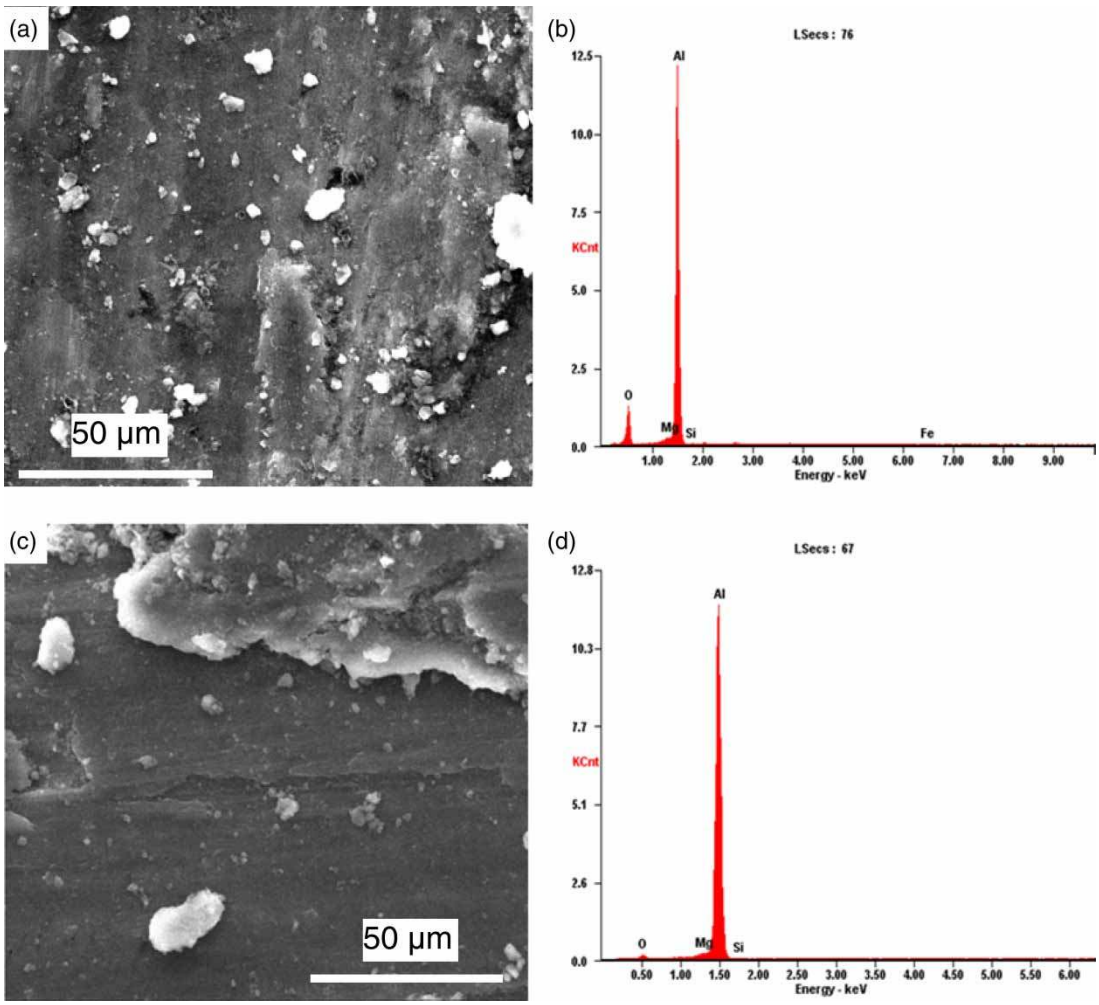

Fig. 8 Scanning electron microscope images and the corresponding EDS spectrum of the worn surface for an applied load, 30 N: (a) and (b) unpeened sample, and (c) and (d) sample peened at 0.5 mm/s

the oxidation that has occurred in the worn surface. The analysis also indicated severe oxidation in the unpeened samples compared to peened sample under all the conditions investigated and the wear is associated with the breaking of the oxide layer. Figure 8 shows the scanning electron microscope image and the corresponding EDS spectrum of the unpeened and sample peened at 0.5 mm/s tested at an applied load, 30 N.

4 CONCLUSIONS

OJP of aluminium alloy, AA6063-T6, which results in surface modification by refining the grain size, induction of compressive residual stress and hardening, influences the sliding friction and wear characteristics. The nozzle-travelling velocity affects the peening pattern, the compressive residual stress induced, grain size, indentation hardness, and surface roughness in aluminium alloys. The surface texture created by the peening process contributes to the reduced coefficient of friction. The high surface strength and associated grain refinement of the treated surface delay the crack initiation and arrest the crack propagation, resulting in the significant improvement in the wear resistance.

REFERENCES

1 **Sahaya Grinspan, A.** and **Gnanamoorthy, R.** A novel surface modification technique for the introduction of compressive residual stress and preliminary studies on Al alloy AA6063. *Surf. Coat. Technol.*, 2006, **201**, 1768–1775.
2 **Sahaya Grinspan, A.** and **Gnanamoorthy, R.** Fatigue behavior of oil jet peened aluminium alloy, AA6063-T6. *Trans. JSME, J. Solid Mech. Mater. Eng.*, 2007, **1**, 875–885.
3 **Sahaya Grinspan, A.** and **Gnanamoorthy, R.** Surface modification and fatigue behavior of high-pressure oil jet peened medium carbon steel, AISI 1040. *Trans. ASME, J. Manuf. Sci. Eng.*, 2007, **129**, 601–606.

4 **Gavgali, M., Totik, Y.,** and **Sadeler, R.** The effects of artificial aging on wear properties of AA 6063 alloy. *Mater. Lett.*, 2003, **57**, 3713–3721.

5 **Mindivan, H., Baydogan, M., Sabri Kayali, E.,** and **Cimenoglu, H.** Wear behavior of 7039 aluminium alloy. *Mater. Charact.*, 2005, **54**, 263–269.

6 **Subramanian, C.** Effects of sliding speed on the unlubricated wear behavior of Al-12.3 wt%Si alloy. *Wear*, 1991, **151**, 97–110.

7 **Somi Reddy, A., Pramila Bai, B. N., Murthy, K. S. S.,** and **Biswas, S. K.** Mechanisms of seizure of aluminium–silicon alloys dry sliding against steel. *Wear*, 1995, **181–183**, 658–667.

8 **Sánchez-Santana, U., Rubio-González, C., Gomez-Rosas, G., Ocaña, J. L., Molpeceres, C., Porro, J.,** and **Morales, M.** Wear and friction of 6061-T6 aluminium alloy treated by laser shock processing. *Wear*, 2006, **260**, 847–854.

9 **Arun Prakash, N., Gnanamoorthy, R.,** and **Kamaraj, M.** Friction and wear behavior of surface nanocrystallized aluminium alloy under dry sliding condition. *Mater. Sci. Eng. B*, 2010, **168**, 176–181. DOI:10.1016/j.mseb.2009.11.011.

10 **Arun Prakash, N., Gnanamoorthy, R.,** and **Kamaraj, M.** Microstructural evolution and mechanical properties of oil jet peened aluminum alloy, AA6063-T6. *Materials and Design*, 2010, **31**, 4066–4075.

11 **Sahaya Grinspan, A.** and **Gnanamoorthy, R.** Surface modification by oil jet peening in Al alloys, AA6063-T6 and AA6061-T4: Residual stress and hardness. *Appl. Surf. Sci.*, 2006, **253**, 997–1005.

12 **Kunaporn, S., Ramulu, M.,** and **Hashish, M.** Mathematical modeling of ultra-high-pressure waterjet peening. *Trans. ASME, J. Eng. Mater. Technol.*, 2005, **127**, 186–191.

13 **Oliver, W. C.** and **Pharr, G. M.** An improved technique for determining hardness and elastic modulus using load and displacement sensing indentation measurements. *J. Mater. Res.*, 1992, **7**, 1564–1583.

14 **Suresh, S.** and **Giannakopoulous, A. E.** A new method for estimating residual stresses by instrumented sharp indentation. *Acta. Mater.*, 1998, **46**, 5755–5767.

APPENDIX

Notation

C_v	coefficient of nozzle
C_1	velocity of sound in oil
C_2	velocity of sound in target material
d_n	nozzle throat diameter (mm)
K	specific wear rate (m^2/N)
P	applied normal load (N)
P_{imp}	impact pressure (MPa)
P_0	operating oil pressure (MPa)
S	sliding distance (m)
SOD	stand-off distance (mm)
t_p	exposure time of the target surface by repeated impacts over a contact area (s)
u	nozzle-travelling velocity (mm/s)
V	wear volume (m^3)
θ	diverging angle of the oil jet droplet (degree)
ρ_1	density of oil (kg/m^3)
ρ_2	density of target material (kg/m^3)